Journal of Hepatocellular Carcinoma

Dovepress

open access to scientific and medical research

Open Access Full Text Article

ORIGINAL RESEARCH

MRI Radiomics Combined with Clinicopathological Factors for Predicting 3-Year Overall Survival of Hepatocellular Carcinoma After Hepatectomy

Fangyuan Kuang[1,2], Yang Gao[3], Qingyun Zhou[4], Chenying Lu[3], Qiaomei Lin[4], Abdullah Al Mamun[5], Junle Pan[6], Shuibo Shi[7], Chaoyong Tu[4,*], Chuxiao Shao[2,*]

[1]School of Medicine, Shaoxing University, Shaoxing, Zhejiang, 312000, People's Republic of China; [2]Department of Hepatopancreatobiliary Surgery, People Hospital of Lishui, The Sixth Affiliated Hospital of Wenzhou Medical University, The First Affiliated Hospital of Lishui University, Lishui, Zhejiang, 323000, People's Republic of China; [3]Department of Radiology, the Fifth Affiliated Hospital of Wenzhou Medical University, Lishui, Zhejiang, 323000, People's Republic of China; [4]Department of Hepatopancreatobiliary Surgery, The Fifth Affiliated Hospital of Wenzhou Medical University, Lishui, Zhejiang, 323000, People's Republic of China; [5]Key Laboratory of Joint Diagnosis and Treatment of Chronic Liver Disease and Liver Cancer of Lishui, The Sixth Affiliated Hospital of Wenzhou Medical University, Lishui People's Hospital, Lishui, Zhejiang, 323000, People's Republic of China; [6]First Academy of Clinical Medicine, Wenzhou Medical University, Wenzhou, Zhejiang, 325000, People's Republic of China; [7]The First Clinical Medical College of Nanchang University, Nanchang City, Jiangxi, 330000, People's Republic of China

*These authors contributed equally to this work

Correspondence: Chaoyong Tu, Department of Hepatopancreatobiliary Surgery, The Fifth Affiliated Hospital of Wenzhou Medical University, Lishui, Zhejiang, 323000, People's Republic of China, Email tcy7409@163.com

Background: A limited number of studies have examined the use of radiomics to predict 3-year overall survival (OS) after hepatectomy in patients with hepatocellular carcinoma (HCC). This study develops 3-year OS prediction models for HCC patients after liver resection using MRI radiomics and clinicopathological factors.

Materials and Methods: A retrospective analysis of 141 patients who underwent surgical resection of HCC was performed. Patients were randomized into two set: the training set (n=98) and the validation set (n=43) including the survival groups (n=111) and non-survival groups (n=30) based on 3-year survival after hepatectomy. Furthermore, x^2 or Fisher's exact test, univariate and multivariate logistic regression analyses were conducted to determine independent clinicopathological risk factors associated with 3-year OS. 1688 quantitative imaging features were extracted from preoperative T2-weighted imaging (T2WI) and contrast-enhanced magnetic resonance imaging (CE-MRI) of arterial phase (AP), portal venous phases (PVP)and delay period (DP). The features were selected using the variance threshold method, the select K best method and the least absolute shrinkage and selection operator (LASSO) algorithm. By using Bernoulli Naive Bayes (BernoulliNB) and Multinomial Naive Bayes (MultinomialNB) classifiers, we constructed models based on the independent clinicopathological factors and Rad-scores. To determine the best model, receiver operating characteristics (ROC) and Delong's test were used. Moreover, calibration curves were used to determine the calibration ability of the model, while decision curve analysis (DCA) was implemented to evaluate its clinical benefit.

Results: The fusion model showed excellent prediction precision with AUC of 0.910 and 0.846 in training and validation set and revealed significant diagnostic accuracy and value in the calibration curve and DCA analysis.

Conclusion: Nomograms based on MRI radiomics and clinicopathological factors have significant predictive value for 3-year OS after hepatectomy and can be used for risk classification.

Keywords: hepatocellular carcinoma, hepatectomy, MRI radiomics

Introduction

Liver cancer, the third most significant cause of cancer fatalities, has drastically affected lives and health globally.[1] Furthermore, the incidence of HCC is estimated to be between 85% and 90% of all primary liver cancers.[2] HCC is being diagnosed at an earlier stage with the advancement of medical technology. Surgical resection may be utilized in the HCC

Received: 26 February 2024
Accepted: 24 June 2024
Published: 18 July 2024

patients of early stage with the aim of achieving curative outcomes. However, it should be noted that only a relatively small percentage of patients undergoing this treatment will eventually experience adequate recovery. Precise prognosis prediction is crucial for developing effective treatment strategies. The risk of HCC cannot be classified or categorized based on the particular patient. Therefore, identifying high-risk patients following HCC requires a practical and consistent methodology.

Several clinicopathological features have been demonstrated to increase predicting the prognosis of HCC. Numerous diagnostic and prognostic models for HCC utilize alpha-fetoprotein (AFP), a widely regarded tumor marker associated with HCC.[3–8] The threshold for pathological alterations associated with HCC is generally defined as >20 ng/mL, and a concentration of >400ng/mL is generally accepted as one of the crucial diagnostic indicators for HCC.[9] KI-67 is a marker of cellular proliferation and an independent predictor of HCC recurrence.[10–12] In addition, KI-67 can indicate tumor biology and determine prognosis.

Previous imaging studies[13–15] have relied on the qualitative assessment of tumor morphology, density and enhancement, which are laborious means of quantifying tumor information and susceptible to misdiagnosis due to the subjective influence of radiologists. Heterogeneous malignancy cells and their microenvironment have been shown to impact tumor biology, which can be examined by imaging. Radiomics, an emerging field, constructs a statistical model using multiple high-dimensional mineable variables derived from medical imaging data to facilitate diagnosis, prognosis and therapy monitoring.

The relationship between MRI-based radiomics, pathology and prognosis in HCC patients is poorly understood. The prognosis of liver cancer patients has not been assessed using MRI-based radiomics. Studies have focused on predicting recurrence-free survival in HCC patients,[3,4,12,16–18] with fewer examining OS.[19] Therefore, this research aims to construct a model using MRI-based radiomics and clinical metrics to predict 3-year OS in HCC patients. The purpose of the model is to facilitate clinical decision-making, treatment strategy and long-term postoperative follow-up. The primary objective of this research is to develop novel prospects for targeted precision therapy.

Materials and Methods

Patients

This retrospective study was approved by the Ethics Committee of Lishui Municipal Central Hospital (Approval No. 2023–720). As this was a retrospective study, informed consent was not required, nor were these decisions in any way detrimental to the rights of the study Patients. The confidentiality of patient data was strictly protected to ensure compliance with all relevant regulations and in line with the Declaration of Helsinki. According to the following inclusion criteria, 141 consecutive patients with liver cancer who underwent hepatectomy in the Department of Hepatobiliary and Pancreatic Surgery of Lishui Central Hospital, Zhejiang Province, China from September 2010 to July 2023 were enrolled: (1) patients who underwent primary radical hepatectomy and were pathologically confirmed to have HCC; (2) histopathological evidence showed no residual neoplastic tissue at the margin of the resection, which is required by R0 resection standards. (3) no lymph node and extrahepatic metastasis; (4) no major vascular invasion; (5) no radiofrequency ablation, transcatheter arterial chemoembolization (TACE) and chemotherapy prior to surgery; (6) patients who underwent enhanced MRI preoperatively. Exclusion criteria were as follows: (1) patients with benign or mixed liver tumors; (2) combined with other malignant tumors; (3) death due to surgical complications; (4) liver transplantation performed during the course of the disease; (5) incomplete clinical or follow-up data. Figure 1 illustrates the procedure for recruiting participants for the study. All patients underwent hepatectomy and pathological evaluation within two weeks of collection of clinical features and MRI examination. We randomly divided eligible patients into two groups in a 7:3 ratio: the training set (n =98) and the validation set (n =43).

Preoperative Clinical Characteristics

Data was collected from the electronic medical record system for the following patients. (1) The basic clinical characteristics of preoperative patients such as age, sex, body mass index (BMI), hypertension and diabetes mellitus; (2) preoperative routine laboratory indexes such as hepatitis B virus (HBV) status, alpha-fetoprotein (AFP), alanine aminotransferase (ALT), aspartate

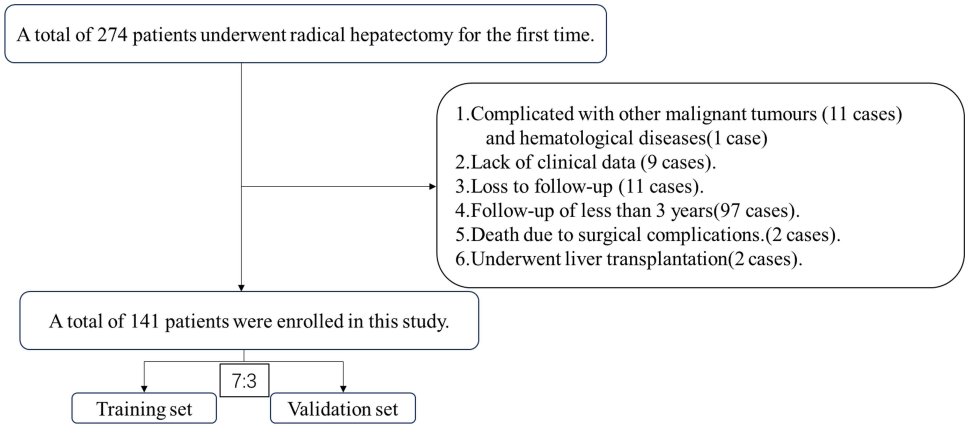

Figure 1 Flow chart for screening patients.

aminotransferase (AST), alkaline phosphatase (ALP), γ-glutamyl transferase (GGT), direct bilirubin (DBIL), total bilirubin (TBIL), prealbumin (PALB), albumin (ALB), white blood cell count (WBC), neutrophil count (NEUT), lym monocyte count (MNC), SII (platelet × neutrophil/lymphocyte), ALBI (0.66 × log10 [bilirubin (μmol/L)] − 0.085 × [albumin (g/L)]); (2) Operation information such as intraoperative blood loss and blood transfusion; (3) pathological information such as tumor number, size, microvascular invasion (MVI), Ki-67; (4) tumor stage was determined based on the Child Pugh stage, the Barcelona Clinic Liver Cancer (BCLC)[20] classification system and the American Joint Committee on cancer's tumor-node-metastasis (TNM)[21] system. Histopathological analysis was performed by a pathologist with 10 years of experience in liver pathology, who was blinded to the radiological and clinical findings. MVI is defined as the microscopic observation of tumor cell nests within the wall of the portal vein, hepatic vein, and peritumoral vessel, lined by a single layer of endothelium.[22] Immunohistochemistry staining for Ki-67 protein was performed. The Ki-67 expression was assessed by noting the percentage of positively stained cells with brownish yellow nuclei,[23] Supplementary Figure 1 shows the immunohistochemical results of MVI and Ki-67.

MRI Procedure

The German Siemens Aheral.5T or Siemens Symphony 1.5T superconducting MRI imaging system was used. MRI scans were performed using a T2-weighted sequence and a multiphase CE-MRI sequence. The T2-weighted sequence parameters were as follows: TR 3500 ms, TE 90 ms, FOV 380 mm × 380 mm, matrix 320 × 320; CE-MRI scans were performed with three-dimensional volume interpolation (3D-VIBE): TR 4.1ms, TE 1.8 ms, FOV: 380 mm × 380 mm, matrix: 320 × 320, thickness 5 mm, gap1 mm. The images of AP, PVP and DP were collected after injecting contrast agent Gd-DTPA (dose 0.1 mmol/kg, flow rate 2 mL/s) for 20–30 s, 60–70 s and 180 s, respectively.

Follow-Up

Patients with HBV were treated with anti-HBV according to protocols. All HCC patients were followed up at 3–6 months post-operatively for the first 2 years. The follow-up frequency was increased to 6–12 months. To detect recurrences of the tumor, liver and renal function, blood parameters and abdominal enhancement CT and chest CT were examined. Abdominal MRI or PET-CT were performed to detect recurrence. OS was assessed from the day of surgery until the time of death or the most recent follow-up.

Image Preprocessing and Tumor Segmentation

We exported T2WI and CE-MRI (AP, PVP and DP) scans in DICOM format from the picture archiving and communication system. MRI images were manually specified by tow radiologist blinded to the clinical information of the patients using Radcloud (http://radcloud.cn). Senior radiologists defined tumor boundaries if the variation was 5%.[24]

Radiomics Feature Extraction

A total of 1688 quantitative imaging features were extracted from MR images. These features were grouped into three groups. Group 1 (first-order statistics) consisted of 126 features that quantitatively indicate the distribution of voxel intensities within the MRI image through commonly used and basic metrics. Group 2 (shape- and size-based features) contained 14 three-dimensional features that reflect the shape and size of the region. We classified 525 textural features into group 3 (texture features) using grey-level run-length and grey-level co-occurrence texture matrices.

Feature Selection and Model Construction

Various image features can be determined using the methods described before. A few features may not be applicable to each task. Therefore, task-specific characteristics selection and dimensionality reduction are important for effective performance. The first step was to select features for each volume of interest. The variance threshold, SelectKBest and least absolute shrinkage and selection operator reduced redundant functions. Next, BernoulliNB and MultinomialNB classifiers were employed to maximize radiomics algorithm discrimination for each sequence and combination to develop the most excellent radiomics model. To create the final fusion model, clinicopathological characteristics were included in the radiomics model and evaluated using ROC and Delong's test. Nomograms were generated from fusion models. Clinical value was assessed using decision curve analysis, whereas nomogram prediction accuracy and differentiation were analyzed using calibration curves.

Statistical Analysis

Categorical variables were represented numerically and proportionately and contrasted using the x^2 or Fisher's exact test. The x^2 test, Fisher's exact test and logistic regression analysis were conducted using SPSS version 23.0, a statistical software developed by IBM Corporation. Furthermore, volume of interest segmentation, feature extraction and model construction processes were performed using the Radcloud platform (http://radcloud.cn/). Manual tumor segmentation, feature extraction, model creation and evaluation comprised the workflow (Figure 2). Finally, we plotted many datasets using R (4.3.1). Extracting and selecting features and performing statistical analysis are addressed in the Supplementary Tables 1–7.

Results

Patient Characteristics

A total of 141 patients (male/female: 123/18; age <60/age>60: 86/55) were included in the final study group and randomly divided into the training set (n = 98) and validation set (n = 43), including the survival groups (n = 111) and non-survival groups (n = 30) based on 3-year survival after hepatectomy. Demographic and clinicopathological characteristics of included patients are shown in Table 1. Both training and validation sets showed no significant difference in characteristics (P = 0.087 to 0.999) including 3-year OS status.

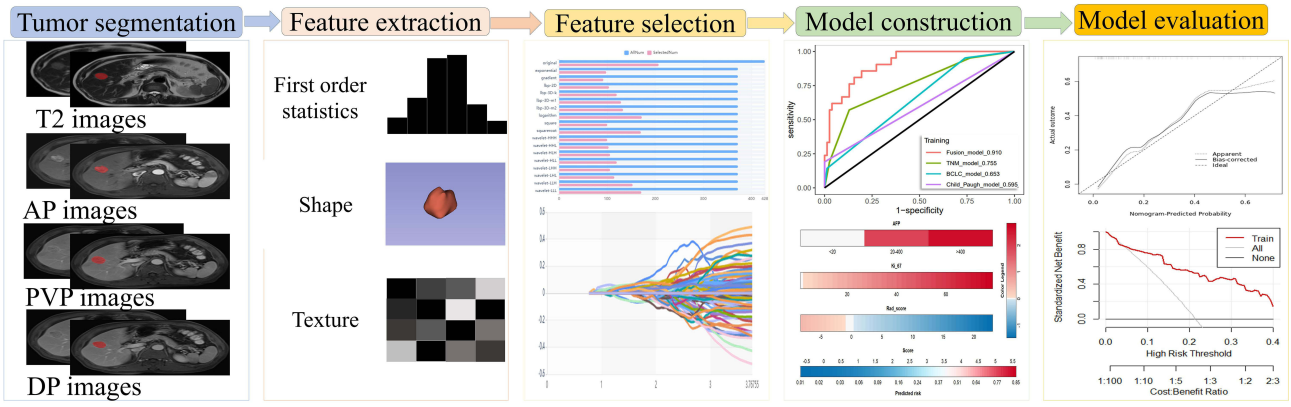

Figure 2 Flowchart of radiomics analysis.

Table 1 Baseline Characteristics of Training and Validation Groups

Characteristics	Total	Training (n = 98)	Validation (n = 43)	P-value
Demographics and history				
3-year OS status				0.947
Survivor	111 (78.7%)	77 (78.6%)	34 (79.1%)	
Non-survivor	30 (21.3%)	21 (21.4%)	9 (20.9%)	
Age, years				0.404
<60	86 (61.0%)	62 (63.3%)	24 (55.8%)	
>60	55 (39.0%)	36 (36.7%)	19 (44.2%)	
Gender				0.414
Male	123 (87.2%)	84 (85.7%)	39 (90.7%)	
Female	18 (12.8%)	14 (14.3%)	4 (9.3%)	
BMI, Kg/m2				0.171
0–18	46 (32.6%)	28 (28.6%)	18 (41.9%)	
18–24	85 (60.3%)	61 (62.2%)	24 (55.8%)	
24+	10 (7.1%)	9 (9.2%)	1 (2.3%)	
HBsAg status				>0.999
Negative	128 (90.8%)	89 (90.8%)	39 (90.7%)	
Positive	13 (9.2%)	9 (9.2%)	4 (9.3%)	
Diabetes				0.247
Absent	130 (92.2%)	104 (93.7%)	26 (86.7%)	
Present	11 (7.8%)	7 (6.3%)	4 (13.3%)	
Hypertension				0.326
Absent	23 (16.3%)	14 (14.3%)	9 (20.9%)	
Present	118 (83.7%)	84 (85.7%)	34 (79.1%)	
Preoperative blood tests				
AFP, ng/mL				0.563
<20	53 (37.6%)	39 (39.8%)	14 (32.6%)	
20–400	44 (31.2%)	31 (31.6%)	13 (30.2%)	
>400	44 (31.2%)	28 (28.6%)	16 (37.2%)	
ALT, IU/L				0.574
<50	35 (24.8%)	23 (23.5%)	12 (27.9%)	
>50	106 (75.2%)	75 (76.5%)	31 (72.1%)	
AST, IU/L				0.965
<40	39 (27.7%)	27 (27.6%)	12 (27.9%)	
>40	102 (72.3%)	71 (72.4%)	31 (72.1%)	
GGT, U/L				0.362
<40	48 (34.0%)	31 (31.6%)	17 (39.5%)	
>40	93 (66.0%)	67 (68.4%)	26 (60.5%)	
ALP, U/L				0.109
0	128 (90.8%)	86 (87.8%)	42 (97.7%)	
1	13 (9.2%)	12 (12.2%)	1 (2.3%)	
DBIL, umol/L	6.3 ± 3.3	6.1 ± 3.2	6.6 ± 3.5	0.426
TBIL, umol/L	15 ± 7	15 ± 7	16 ± 8	0.44
PALB	207 ± 68	206 ± 62	210 ± 79	0.774
ALB, g/L	39.7 ± 4.3	39.7 ± 4.2	39.7 ± 4.7	>0.999
WBC, $\times 10^9$/L	5.55 ± 2.37	5.38 ± 2.48	5.94 ± 2.09	0.167
NEUT, $\times 10^9$/L	3.26 ± 1.52	3.12 ± 1.40	3.59 ± 1.74	0.119
Lym, $\times 10^9$/L	1.68 ± 1.68	1.67 ± 1.98	1.70 ± 0.61	0.901
MNC, $\times 10^9$/L	0.49 ± 0.48	0.50 ± 0.57	0.48 ± 0.19	0.714
SII	321 ± 253	303 ± 252	361 ± 256	0.213
ALBI	−2.62 ± 0.38	−2.63 ± 0.36	−2.61 ± 0.42	0.809

(*Continued*)

Table 1 (Continued).

Characteristics	Total	Training (n = 98)	Validation (n = 43)	P-value
Preoperative imaging				
Largest tumor size, cm	4.45 ± 3.17	4.46 ± 3.50	4.43 ± 2.31	0.961
Tumor number				0.087
Solitary	123 (87.2%)	90 (91.8%)	35 (81.4%)	
Multiple	18 (12.8%)	8 (8.2%)	8 (18.6%)	
Operative results				
Intraoperative bleeding				0.948
<400	76 (53.9%)	53 (54.1%)	23 (53.5%)	
>400	65 (46.1%)	45 (45.9%)	20 (46.5%)	
Blood transfusion				0.581
<400	87 (61.7%)	59 (60.2%)	28 (65.1%)	
>400	54 (38.3%)	39 (39.8%)	15 (34.9%)	
Pathology				
KI-67	32 ± 20	31 ± 20	34 ± 20	0.276
MVI				0.408
Absent	111 (78.7%)	79 (80.6%)	32 (74.4%)	
Present	30 (21.3%)	19 (19.4%)	11 (25.6%)	
Tumor stage				
BCLC-stage				0.333
0	27 (19.1%)	21 (21.4%)	6 (14.0%)	
1	106 (75.2%)	73 (74.5%)	33 (76.7%)	
2	8 (5.7%)	4 (4.1%)	4 (9.3%)	
TNM-stage				0.175
T1a	25 (17.7%)	19 (19.4%)	6 (14.0%)	
T1b	79 (56.4%)	57 (58.2%)	22 (52.4%)	
T2	30 (21.4%)	16 (16.3%)	14 (33.3%)	
T3	7 (5.0%)	6 (6.1%)	1 (2.4%)	
Child Pugh stage				>0.999
A	135 (95.7%)	94 (95.9%)	41 (95.3%)	
B	6 (4.3%)	4 (4.1%)	2 (4.7%)	

Abbreviations: BMI, body mass index; HBsAg, hepatitis B surface antigen; AFP, alpha-fetoprotein; ALT, alanine aminotransferase; AST, aspartate aminotransferase; GGT, γ-glutamyl transpeptidase; ALP, alkaline phosphatase; DBIL, direct bilirubin; TBIL, total bilirubin; PALB, prealbumin; ALB, albumin; SII= platelet × neutrophil/lymphocyte; ALBI=0.66 × log10 [bilirubin (μmol/L)] − 0.085 × [albumin (g/L)]; KI-67; MVI, microvascular invasion; BCLC, Barcelona Clinic Liver Cancer; TNM, the American Joint Committee on Cancer tumor-node-metastasis system.

Correlation Between Clinical Factors and 3-Year OS in Patients

Univariate analysis revealed that five factors (AFP, Lym, largest tumor size, KI-67 and MVI) were significantly correlated with prognosis ($P < 0.05$). Multivariate analysis confirmed that KI-67 ($p = 0.019$, OR = 1.030, 95%CI: 1.005–1.056) and AFP ($p = 0.002$, OR = 2.887, 95%CI: 1.492–5.547) were independent risk factors for 3-year OS (Table 2).

Predictive Performance of Radiomics Signatures from Different MRI Sequences and Classifiers

The Results of MRI sequences for variance threshold, SelectKBest, and LASSO are presented in Supplementary Tables 1 and the Table 3 shows the predictive performance of imaging radiomics features extracted from different MR sequences by various classifiers. We found the fusion radiomics model (T2+AP+PVP+DP) with the MultinomialNB classifier highly predictive in both the training and validation sets. The AUC for the training set was 0.899 (95% CI: 0.817–0.981) and for the validation set was 0.768 (95% CI: 0.615–0.921). We then incorporated independent clinical factors (KI-67 and AFP) into the fusion radiomics model (T2+AP+PVP+DP) to construct a predictive model using the variance

Table 2 Clinical and Pathological Factors for 3-Year Survival in Patients with HCC

Variables	Univariate Analysis Regression		Multi-Variate Analysis Regression	
	OR (95% CI)	P-value	OR (95% CI)	P-value
Demographics and history				
Age, years				
<60/>60	11.34 (0.493–2.613)	0.767		
Gender				
Female/Male	0.361 (0.126–1.033)	0.058		
BMI, Kg/m2		0.713		
18–24/0-18	0.813 (0.159–4.141)	0.803		
18–24/24+	0.684 (0.274–1.704)	0.415		
HBsAg				
Negative/Positive	1.950 (0.778–4.887)	0.237		
Diabetes				
Absent/Present	2.286 (0.622–8.399)	0.213		
Hypertension				
Absent/Present	0.506 (0.140–1.832)	0.299		
Preoperative blood tests				
AFP, ng/mL				
<20/20-400/>400	3.525 (1.931–6.436)	<0.001	2.887 (1.492–5.547)	0.002
ALT, IU/L				
<50/>50	1.401 (0.572–3.432)	0.461		
AST, IU/L				
<40/>40	1.414 (0.593–3.372)	0.435		
GGT, U/L				
<40/>40	1.924 (0.760–4.876)	0.168		
ALP, U/L				
<150/>150	1.122 (0.289–4.365)	0.868		
DBIL, umol/L	0.988 (0.883–1.128)	0.973		
TBIL, umol/L	0.972 (0.913–1.035)	0.373		
PALB	0.994 (0.987–1.000)	0.064		
ALB, g/L	0.923 (0.837–1.018)	0.108		
WBC, 10^9/L	0.888 (0.713–1.105)	0.287		
NEUT, $\times 10^9$/L	0.989 (0.757–1.292)	0.934		
Lym, $\times 10^9$/L	0.444 (0.210–0.942)	0.034		
MNC, $\times 10^9$/L	0.703 (0.163–3.038)	0.637		
SII	1.001 (0.999–1.002)	0.368		
ALBI	2.087 (0.699–6.233)	0.187		
Preoperative imaging				
Largest tumor size, cm	1.149 (1.014–1.298)	0.025		
Tumor number				
Solitary/Multiple	2.525 (0.836–7.629)	0.101		
Operative results				
Intraoperative bleeding, mL				
<400/>400	1.220 (0.544–2.736)	0.629		
Blood transfusion, mL				
<400/>400	1.095 (0.480–2.499)	0.829		
Pathology				
KI-67	1.039 (1.017–1.062)	<0.001	1.030 (1.005–1.056)	0.019
MVI				
Absent/Present	3.444 (1.418–8.370)	0.006		

Abbreviations: BMI, body mass index; HBsAg, hepatitis B surface antigen; AFP, alpha-fetoprotein; ALT, alanine aminotransferase; AST, aspartate aminotransferase; GGT, γ-glutamyl transpeptidase; ALP, alkaline phosphatase; DBIL, direct bilirubin; TBIL, total bilirubin; PALB, prealbumin; ALB, albumin; SII= platelet × neutrophil/lymphocyte; ALBI=0.66 × log10 [bilirubin (μmol/L)] − 0.085 × [albumin (g/L)]; KI-67; MVI, microvascular invasion.

Table 3 The Predictive Performance of Imaging Radiomics Features E×tracted from MR Sequences by Various Classifiers

Models	Classifiers	Training Set			Validation Set		
		AUC (95% CI)	Sen	Spe	AUC (95% CI)	Sen	Spe
T2							
	BernoulliNB	0.771 (0.657–0.885)	0.670	0.690	0.735 (0.598–0.872)	0.890	0.560
	MultinomialNB	0.614 (0.495–0.733)	0.620	0.550	0.703 (0.538–0.868)	0.780	0.500
AP							
	BernoulliNB	0.775 (0.656–0.894)	0.620	0.640	0.734 (0.551–0.917)	0.670	0.680
	MultinomialNB	0.769 (0.656–0.882)	0.670	0.730	0.722 (0.539–0.905)	0.670	0.650
PVP							
	BernoulliNB	0.698 (0.580–0.816)	0.620	0.620	0.740 (0.557–0.923)	0.670	0.650
	MultinomialNB	0.725 (0.605–0.845)	0.620	0.660	0.807 (0.632–0.982)	0.670	0.710
DP							
	BernoulliNB	0.698 (0.580–0.816)	0.620	0.620	0.740 (0.557–0.923)	0.670	0.650
	MultinomialNB	0.725 (0.605–0.845)	0.620	0.660	0.807 (0.632–0.982)	0.670	0.710
T2+AP+PVP+DP							
	BernoulliNB	0.928 (0.843–1.000)	0.860	0.860	0.693 (0.515–0.871)	0.330	0.790
	MultinomialNB	0.899 (0.817–0.981)	0.860	0.860	0.768 (0.615–0.921)	0.780	0.820
T2+AP+PVP+DP+AFP+KI-67							
	BernoulliNB	0.947 (0.864–1.000)	0.860	0.880	0.735 (0.547–0.923)	0.560	0.790
	MultinomialNB	0.910 (0.823–0.997)	0.860	0.810	0.846 (0.687–1.000)	0.780	0.710

Abbreviations: AUC, area under receiver operating characteristic curve; CI, confidence interval; Sen, sensitivity; Spe, specificity; BernoulliNB, Bernoulli Naive Bayes; MultinomialNB, Multinomial Naive Bayes; T2, T2-weighted imaging; AP, arterial phase; PVP, portal venous phases; DP, delay period.

threshold, SelectKBest and LASSO MultinomialNB. We first selected 2299 features from 6752 features using the variance threshold method, then 882 using select K best and 18 using LASSO. Figure 3 displays the model construction, while the other models can be found in the Supplementary Tables 2–7. The fusion model demonstrated superior predictive accuracy with an AUC of 0.910 (95% CI: 0.823–0.997) in the training dataset and 0.846 (95% CI: 0.687-1.000) in the validation set. The fusion model outperformed the other model in identifying 3-year OS status in the training set (T2 or PVP or DP; MultinomialNB or BernoulliNB classifier) or validation set (T2+AP+PVP+DP by MultinomialNB or BernoulliNB classifier; T2+AP+PVP+DP+AFP+Ki-67 by BernoulliNB classifier) (DeLong's test, $P < 0.05$). Although there was no statistically significant difference in identifying 3-year OS status between the training set (fusion model) and the training set (AP; MultinomialNB classifier) (DeLong's test, $P = 0.066$) or (BernoulliNB classifier) (DeLong's test, $P = 0.062$), it was close to thresholds. Given all the above, we finally selected the fusion model as our best model. Furthermore, the fusion model outperformed BCLC, TNM and Child Pugh models in 3-year OS prediction (DeLong's test, $P < 0.05$) (Figure 4).

3-Year OS Predictive Nomogram Construction and Evaluation

Clinicopathological and radiomics predictions were used to develop a 3-year OS model using AFP, Ki-67 and R-score risk factors. More importantly, Figure 5 shows the visual presentation of this model with R-score, AFP level and Ki-67. The calibration curves indicate that the predicted and actual 3-year OS in the training set are similar (Figure 6). The nomogram provided superior clinical performance for predicting 3-year OS in the training and validation set (Figure 7).

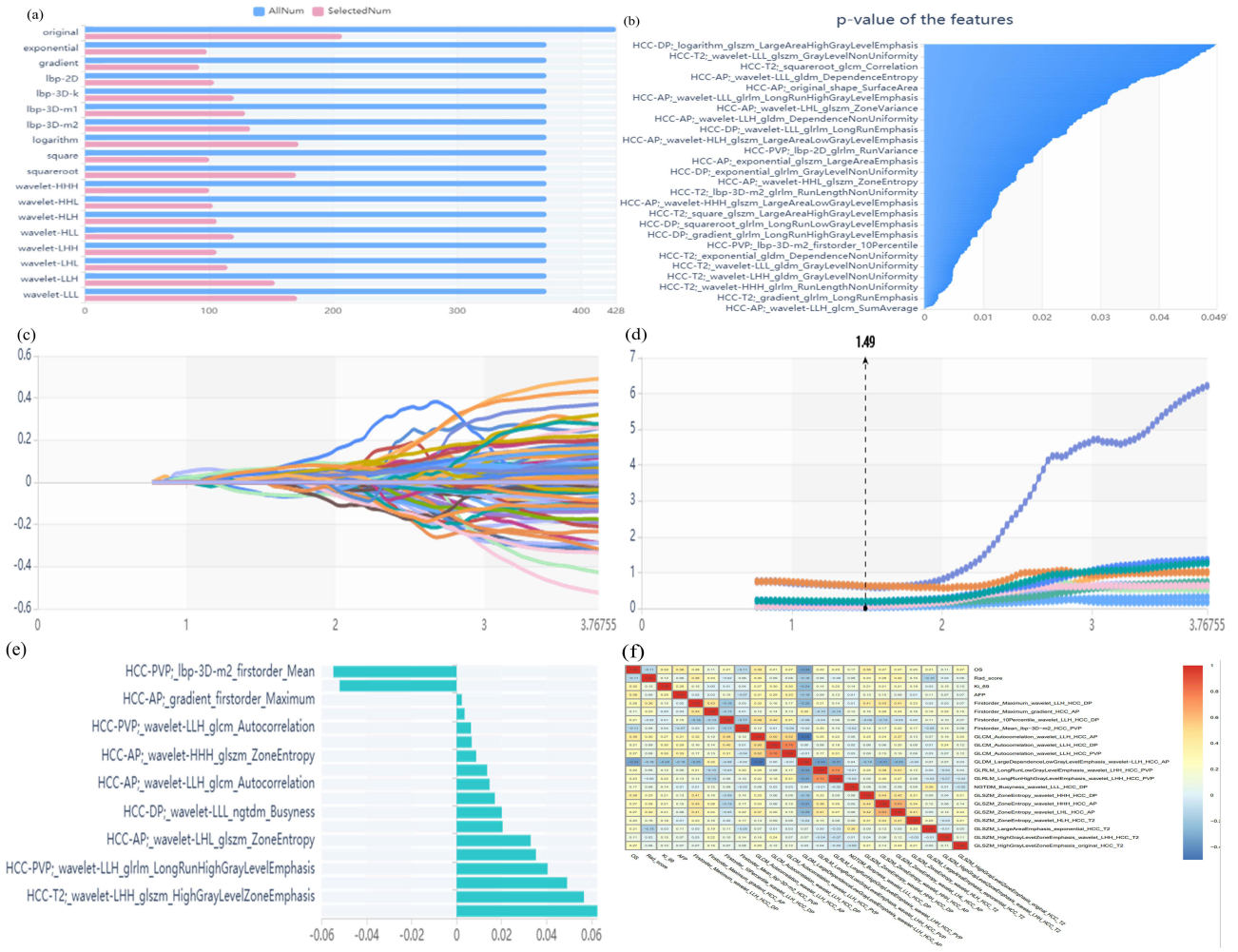

Figure 3 The construction process of the fusion model. (**a**) Variance threshold on feature select. (**b**) Select K best on feature select. (**c**) Lasso algorithm on feature select. (**d**) Lasso path-; MSE path. coefficients in Lass model. Coefficients in the Lasso model. (**e**) Using the Lasso model, 18 features which are correspond to the optimal alpha value were selected. (**f**) Heatmap depicting the correlation coefficient matrix in the radiomics model.

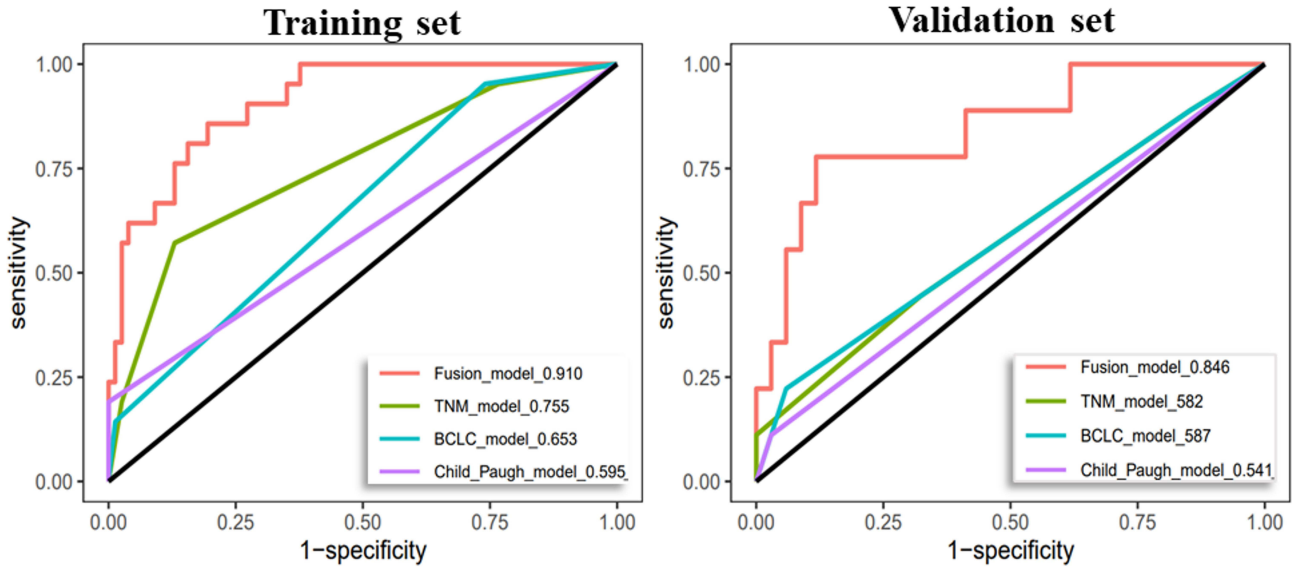

Figure 4 The ROC curve of different models predicts 3-year OS.
Abbreviations: TNM, the American Joint Committee on Cancer tumor-node-metastasis system; BCLC, Barcelona Clinic Liver Cancer.

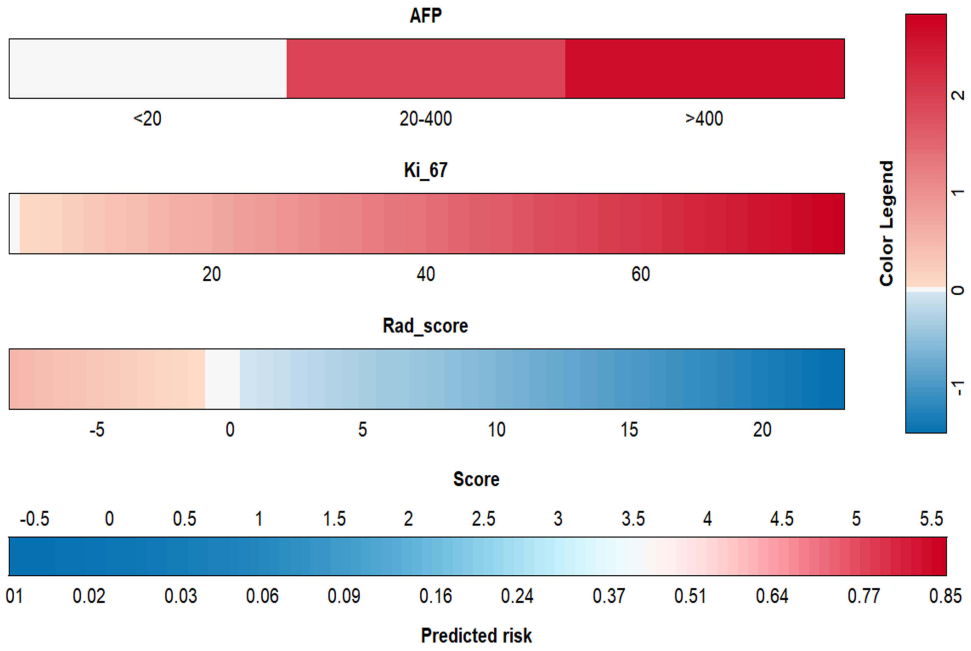

Figure 5 Nomograms for predicting the 3-year OS of HCC patients.

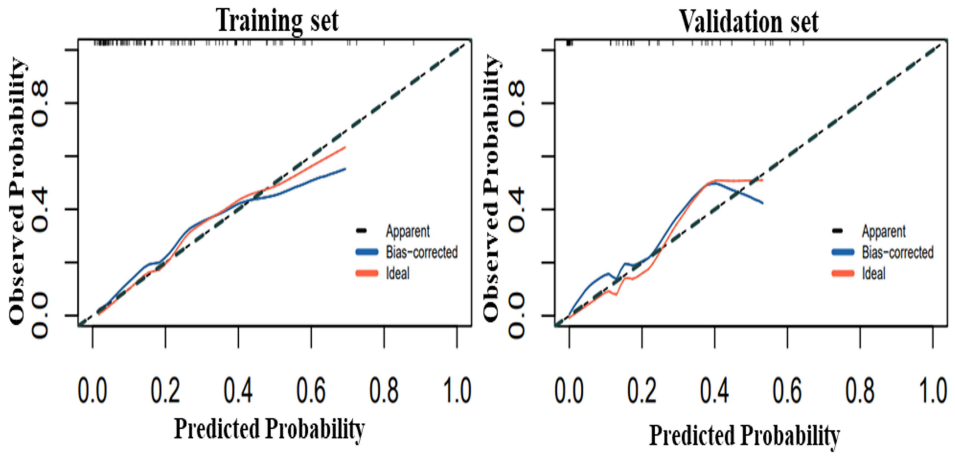

Figure 6 Calibration curves for training and validation sets.

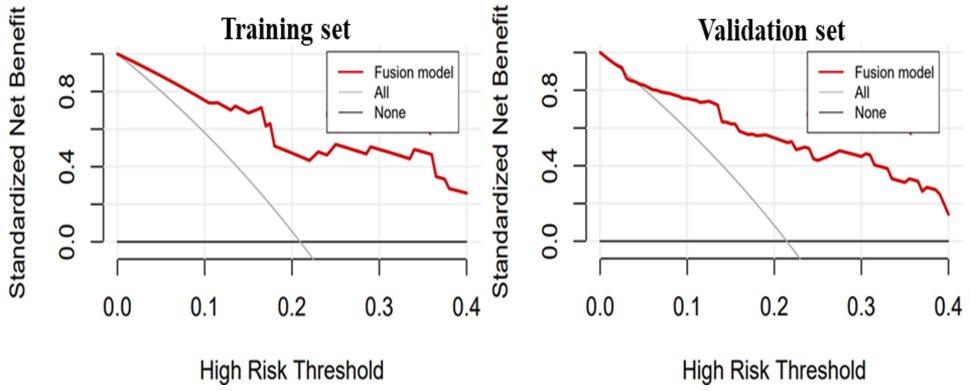

Figure 7 Decision curves for training and validation sets.

Discussion

Based on MRI radiomics and clinicopathological information, a predictive model was developed for HCC patients of 3-year OS status after hepatectomy. Based on this model, we derived excellent and stable biases of 3-year OS in HCC patients, which is essential for timely postoperative intervention and improves long-term survival. Furthermore, it can be used for the rapid delivery of postoperative interventions and screening suitable participants for clinical trials involving postoperative treatments is crucial in enhancing long-term survival. To the best of our knowledge, predictive models based on MRI radiomics scores and clinicopathology data have not been used to estimate the 3-year OS of HCC patients who underwent hepatic resection.

MRI is more effective than CT for detecting and predicting the prognosis of early-stage HCC, which can appear at multiple parameters and sequences.[25] The method has evolved into primary imaging and standard preoperative examinations for HCC.[26] Several MRI-based radiomics models have been developed to enhance the diagnosis and prognosis of patients with HCC. Kim et al[3] developed a clinicopathological-like recurrence prediction model using CE MRI data from 167 patients, exhibiting clinical significance. Furthermore, a radiomics nomogram developed by Zhang et al[4] to predict HCC recurrence combined with traditional clinical radiology risk factors performed better than conventional nomograms and demonstrated the importance of MRI radiomics. A meta-analysis[27] of 15 studies involving 981 patients indicates that MRI radiomics holds high accuracy in predicting MVI of HCC and can be considered a non-invasive method for evaluating the presence of MVI in HCC patients. Zhang et al[28] assessed MRI scans of 136 primary liver cancer patients and found that radiomics characteristics were independently associated with OS of distinct pathological types. Different MRI sequences contain different information and possess varying degrees of predictive efficacy for progression of HCC. Wang et al[19] established an MRI-based radiomics model to predict the 5-year OS of HCC patients. It was found that the dynamic contrast-enhanced imaging sequence showed the highest level of predictive accuracy.

An extensive effort was made by comparing different sequences and classifiers, our study found that the fusion model fusing T2, AP, PVP, DP sequences and independent clinicopathological factors of AFP and Ki-67 showed superior predictive capability. T2WI shows tumor spatial dimension and AP, PVP and DP sequences indicate tumor blood vessel and cell activity. Therefore, fusion radiomic models utilizing T2, AP, PVP and DP sequences may precisely exhibit tumor characteristics, improving diagnostic and therapeutic outcomes. The multivariate analysis showed that KI-67 and AFP were independent risk factors for 3-year OS (Table 2). The 18 radiomatic features of the fusion radiomic model (4 T2 features; 6 AP features; 4 PVP features; 4 DP features) implied tumor biological behaviour and tumor microenvironment. The reason why the AP sequences extracted the most features may be that the hepatic artery serves as the primary source of HCC supply and the AP sequence could more clearly reflect microvasculature alterations of HCC. Furthermore, HCC is a solid tumor rich in blood vessels and angiogenesis plays a significant role in its prognosis.[29] Arizumi et al[30] demonstrated that decreased arterial enhancement during sorafenib treatment was associated with the OS of HCC patients. Zhu et al[31] found that PVP and DP were less predictive than AP. GLZM_ZoneEntropy is the zone entropy in the gray level size zone matrix, which is a texture feature. Higher values indicate more significant texture heterogeneity. Intriguingly, we found that GLSZM_ZoneEntropy in T2, AP and DP sequences are all positively associated with 3-year OS in HCC patients. Accordingly, our findings are in line with the widely accepted cognitive belief that an increase in texture heterogeneity signifies a poor prognosis.[32]

In this study, AFP and KI-67 were independent clinical and pathological risk factors of OS. Consistent with previous research, these clinicopathologic factors have been established as effective predictors of clinical outcomes.[6,10–13,28] The study results indicate no notable correlation between MVI, tumor number, tumor size and survival outcomes. In this study, the relatively short follow-up period and the limited number of cases could explain this observation.

Advantages

This was the first study to combine clinical, pathological and MRI texture features to predict 3-year postoperative OS in HCC patients. Their predictive performance was improved than the BCLC stage, TNM stage and Child-Pugh class. Second, different machine learning methods were utilized to compare training and validation set to improve model

accuracy and objectivity. This study mainly established techniques and methodologies for computer-aided and artificial intelligence analysis to predict 3-year postoperative OS in patients with HCC. We developed a nomogram to predict the 3-year OS of HCC patients using clinicopathological and radiomics factors.

Limitations

There are several limitations in our research. Specifically, selection bias was unpredictable in a single-center retrospective analysis with a small sample size. We analyzed MRI sequences using different classifiers for more detail, but we needed external validation with larger datasets from other facilities. Manual segmentation was employed for selection, which is more precise than semiautomatic and automatic segmentation. However, unclear image borders or subjective errors can result in segmentation errors, which makes subjectivity invariable. Furthermore, retreatment following recurrence and other factors can have a negative impact on 3-year OS prediction.

Conclusion

In summary, our predictive model for the 3-year OS of HCC after hepatectomy using MRI radiomics signatures and clinicopathological variables showed promising findings. Therefore, our findings reveal that this nomogram model may improve clinical decision-making and post-surgery surveillance.

Acknowledgments

We appreciate the Radcloud platform and Home for Researchers editorial team (www.home-for-researchers.com) for language editing service, as well as all of the individuals who participated in these studies and each of the researchers and technicians who made this work possible.

Funding

This study was supported by the Key Research & Development Plan of Zhejiang Province (2024C03171) the projects of Lishui Key Research and Development Plan in Zhejiang Province (2022ZDYF08).

Disclosure

The authors report no conflicts of interest in this work.

References

1. Siegel RL, Miller KD, Fuchs HE, et al. Cancer Statistics, 2021. *CA Cancer J Clin*. 2021;71(1):7–33. doi:10.3322/caac.21654
2. Li Q, Zhu H. Donafenib treatment for hepatocellular carcinoma. *Medicine*. 2021;100(25). doi:10.1097/md.0000000000026373
3. Kim S, Shin J, Kim D-Y, et al. Radiomics on gadoxetic acid–enhanced magnetic resonance imaging for prediction of postoperative early and late recurrence of single hepatocellular carcinoma. *Clin Cancer Res*. 2019;25(13):3847–3855. doi:10.1158/1078-0432.Ccr-18-2861
4. Zhang Z, Jiang H, Chen J, et al. Hepatocellular carcinoma: radiomics nomogram on gadoxetic acid-enhanced MR imaging for early postoperative recurrence prediction. *Cancer Imaging*. 2019;19(1). doi:10.1186/s40644-019-0209-5
5. Hu J, Wang N, Yang Y, et al. Diagnostic value of alpha-fetoprotein combined with neutrophil-to-lymphocyte ratio for hepatocellular carcinoma. *BMC Gastroenterol*. 2018;18(1):186. doi:10.1186/s12876-018-0908-6
6. Tzartzeva K, Obi J, Rich NE, et al. Surveillance imaging and alpha fetoprotein for early detection of hepatocellular carcinoma in patients with cirrhosis: a meta-analysis. *Gastroenterology*. 2018;154(6):1706–1718e1701. doi:10.1053/j.gastro.2018.01.064
7. Ding Y, Liu K, Xu Y, et al. Combination of inflammatory score/liver function and AFP improves the diagnostic accuracy of HBV-related hepatocellular carcinoma. *Cancer Med*. 2020;9(9):3057–3069. doi:10.1002/cam4.2968
8. Ozdemir F, Baskiran A. The importance of AFP in liver transplantation for HCC. *J Gastrointest Cancer*. 2020;51(4):1127–1132. doi:10.1007/s12029-020-00486-w
9. Qian L, Liang Z, Wang Z, et al. Cellular gp96 upregulates AFP expression by blocking NR5A2 SUMOylation and ubiquitination in hepatocellular carcinoma. *J Mol Cell Biol*. 2023;15(5). doi:10.1093/jmcb/mjad027
10. Cao Y, Ke R, Wang S, et al. DNA topoisomerase IIα and Ki67 are prognostic factors in patients with hepatocellular carcinoma. *Oncol Lett*. 2017;13(6):4109–4116. doi:10.3892/ol.2017.5999
11. H-H L, L-N Q, Ma L, et al. Effect of KI-67 positive cellular index on prognosis after hepatectomy in Barcelona clinic liver cancer stage A and B hepatocellular carcinoma with microvascular invasion. *Onco Targets Ther*. 2018;11:4747–4754. doi:10.2147/ott.S165244
12. Zhang X, Wu Z, Peng Y, et al. Correlationship between Ki67, VEGF, and p53 and hepatocellular carcinoma recurrence in liver transplant patients. *Biomed Res. Int.* 2021;2021:1–7. doi:10.1155/2021/6651397
13. Zhang L, Kuang S, Chen J, et al. The role of preoperative dynamic contrast-enhanced 3.0-T MR imaging in predicting early recurrence in patients with early-stage hepatocellular carcinomas after curative resection. *Front Oncol*. 2019;9:1336. doi:10.3389/fonc.2019.01336

14. Min JH, Lee MW, Park HS, et al. Interobserver variability and diagnostic performance of gadoxetic acid-enhanced MRI for predicting microvascular invasion in hepatocellular carcinoma. *Radiology*. 2020;297(3):573–581. doi:10.1148/radiol.2020201940
15. Song L, Li J, Luo Y. The importance of a nonsmooth tumor margin and incomplete tumor capsule in predicting HCC microvascular invasion on preoperative imaging examination: a systematic review and meta-analysis. *Clin Imaging*. 2021;76:77–82. doi:10.1016/j.clinimag.2020.11.057
16. Hui TCH, Chuah TK, Low HM, et al. Predicting early recurrence of hepatocellular carcinoma with texture analysis of preoperative MRI: a radiomics study. *Clin Radiol*. 2018;73(12):1056.e1011–1056.e1016. doi:10.1016/j.crad.2018.07.109
17. Yu Y, Fan Y, Wang X, et al. Gd-EOB-DTPA-enhanced MRI radiomics to predict vessels encapsulating tumor clusters (VETC) and patient prognosis in hepatocellular carcinoma. *Eur Radiol*. 2021;32(2):959–970. doi:10.1007/s00330-021-08250-9
18. Wang L, Feng B, Wang S, et al. Diagnostic value of whole-tumor apparent diffusion coefficient map radiomics analysis in predicting early recurrence of solitary hepatocellular carcinoma≤5 cm. *Abdom Radiol*. 2022;47(9):3290–3300. doi:10.1007/s00261-022-03582-6
19. Wang X-H, Long L-H, Cui Y, et al. MRI-based radiomics model for preoperative prediction of 5-year survival in patients with hepatocellular carcinoma. *Br J Cancer*. 2020;122(7):978–985. doi:10.1038/s41416-019-0706-0
20. Forner A, Reig M, Bruix J. Hepatocellular carcinoma. *Lancet*. 2018;391(10127):1301–1314. doi:10.1016/S0140-6736(18)30010-2
21. Wei YZ, Huang YQ, Zeng SY, et al. 基于SEER数据库第8版肝癌AJCC分期的验证及改良 [Validation and modification of AJCC 8th edition staging system for hepatocellular carcinoma--analysis based on SEER database]. *Zhonghua Yi Xue Za Zhi*. 2021;101(28):2216–2222. Chinese. doi:10.3760/cma.j.cn112137-20201231-03527
22. Xia TY, Zhou ZH, Meng XP, et al. Predicting microvascular invasion in hepatocellular carcinoma using CT-based radiomics model. *Radiology*. 2023;307(4):e222729. doi:10.1148/radiol.222729
23. Hu X, Zhou J, Li Y, et al. Added value of viscoelasticity for MRI-Based Prediction of Ki-67 expression of hepatocellular carcinoma using a deep learning combined radiomics (DLCR) model. *Cancers*. 2022;14(11):2575. doi:10.3390/cancers14112575
24. Lambin P, Rios-Velazquez E, Leijenaar R, et al. Radiomics: extracting more information from medical images using advanced feature analysis. *Eur J Cancer*. 2012;48(4):441–446. doi:10.1016/j.ejca.2011.11.036
25. Zech CJ, Ba-Ssalamah A, Berg T, et al. Consensus report from the 8th international forum for liver magnetic resonance imaging. *Eur Radiol*. 2020;30(1):370–382. doi:10.1007/s00330-019-06369-4
26. Koh DM, Ba-Ssalamah A, Brancatelli G, et al. Consensus report from the 9(th) international forum for liver magnetic resonance imaging: applications of gadoxetic acid-enhanced imaging. *Eur Radiol*. 2021;31(8):5615–5628. doi:10.1007/s00330-020-07637-4
27. Liang G, Yu W, Liu S, et al. The diagnostic performance of radiomics-based MRI in predicting microvascular invasion in hepatocellular carcinoma: a meta-analysis. *Front Oncol*. 2022;12:960944. doi:10.3389/fonc.2022.960944
28. Zhang J, Wang X, Zhang L, et al. Radiomics predict postoperative survival of patients with primary liver cancer with different pathological types. *Ann Transl Med*. 2020;8(13):820. doi:10.21037/atm-19-4668
29. Zhen Z, Shen Z, Hu Y, et al. Screening and identification of angiogenesis-related genes as potential novel prognostic biomarkers of hepatocellular carcinoma through bioinformatics analysis. *Aging*. 2021;13(13):17707–17733. doi:10.18632/aging.203260
30. Arizumi T, Ueshima K, Chishina H, et al. Decreased blood flow after sorafenib administration is an imaging biomarker to predict overall survival in patients with advanced hepatocellular carcinoma. *Dig Dis*. 2014;32(6):733–739. doi:10.1159/000368013
31. Zhu YJ, Feng B, Wang S, et al. Model-based three-dimensional texture analysis of contrast-enhanced magnetic resonance imaging as a potential tool for preoperative prediction of microvascular invasion in hepatocellular carcinoma. *Oncol Lett*. 2019;18(1):720–732. doi:10.3892/ol.2019.10378
32. Lubner MG, Smith AD, Sandrasegaran K, et al. CT texture analysis: definitions, applications, biologic correlates, and challenges. *Radiographics*. 2017;37(5):1483–1503. doi:10.1148/rg.2017170056